

Lepton capture rates due to isotopes of vanadium in astrophysical environment

Ramoona Shehzadi¹ • Jameel-Un Nabi² • Fakeha Farooq¹

Abstract Lepton (electron and positron) capture rates on iron-regime nuclei are an essential element for modeling the late stages of progression of massive stars that become core collapse and thermonuclear supernova. As per previous simulation studies, lepton capture (LC) rates on isotopes of vanadium are believed to have a substantial effect in regulating the Y_e (lepton to baryon fraction) during the final evolutionary phases. The present work involves the calculation of lepton capture rates for 22 isotopes of vanadium by making use of the proton-neutron (pn-) quasiparticle random phase approximation (QRPA) model. The covered mass range is from $A = 43$ to 64 . The LC rates have been computed over stellar densities ranging from 10^1 to 10^{11} (g/cm^3) and for the temperature range $10^7 - 3 \times 10^{10}$ (K). A comparison of our calculated LC rates to the rates computed using other models (IPM and LSSM) has also been presented. As compared to the rates calculated by other models, pn-QRPA rates at high temperature (3×10^{10} K) are larger by 1-2 orders of magnitude.

Keywords Lepton capture rates; pn-QRPA model; Gamow-Teller transitions; core collapse.

Ramoona Shehzadi
Jameel-Un Nabi
Fakeha Farooq

¹Department of Physics, University of the Punjab, Lahore, Pakistan.

²Faculty of Engineering Sciences (FES), GIK Institute of Engineering Sciences and Technology, Topi 23640, Khyber Pakhtunkhwa, Pakistan.

¹Corresponding author email : ramoona.physics@pu.edu.pk

1 Introduction

Massive stars make headway towards core-collapse (Type II) supernova by passing through hydrostatic and explosive nuclear burning phases (Burbidge et al. 1957; Bethe 1990; Rauscher et al. 2002; Busso et al. 1999). In the hydrostatic phase, successive burning of each layer of the star's core contracts the core. Consequently, temperature, density and mass of the core increases. At enough high densities, under the Chandrasekhar mass limit ($\sim 1.5 M_{\odot}$), electron degeneracy pressure resists further shrinking of the core and battles against its collapse. Beyond the Chandrasekhar limit, weak-decay processes, namely; β -decays and lepton captures significantly affect the star's life cycle. Especially the lepton captures (LC), including electron captures (EC) and positron captures (PC), have considerable role in the pre-supernova phases of stellar development (Bethe et al. 1979; Nabi et al. 2007).

During the late evolution stages, star's atmospheric temperature approaches around $\sim 10^9$ K, which leads to a considerable rise in the Fermi energy, E_f , of the degenerate gas. This favors the capture of electrons to heavy nuclei and free protons. The capturing processes lower the electron density within the core and become a cause to reduce Y_e (lepton to baryon ratio) and produce neutrinos. For matter densities up to $\sim 10^{11}$ g/cm^3 , these neutrinos escape the star taking away energy and result in reduction of the entropy of the core (Heger et al. 2001). Thus, the core entropy, Y_e , and Chandrasekhar mass (proportional to Y_e) are controlled by the LC processes (Langanke et al. 2003). These factors mainly decide the dynamical behavior of the collapsing of the core. During the final evolutionary pre-supernova stage, the core is thrust towards collapse. LC rates thus play a decisive part in the modeling of Type II supernova as well as in the dynamics of bounce shock (Hix et al. 2003). Primarily, EC rates

are requisite for the simulation of dynamical evolution of supernovae. In addition, PC rates are of fundamental significance in the stellar environment (Suzuki et al. 2016; Nabi et al. 2007). PC weak rates are appreciable at low density (in the range of $10 - 10^6 \text{ g/cm}^3$) and high temperature regions. On contrary, for high density (especially at relatively low temperature) EC wins over PC (Nabi et al. 2017).

LC weak processes are mainly ruled by the Gamow-Teller (GT) transition strengths in the late stages of star's evolution. GT properties of Fe-peak nuclei are therefore of primary importance in supernovae (Fuller et al. 1980, 1982a, 1982b, 1985). An accurate determination of the weak rates needs detailed knowledge of GT transition strengths in EC (GT_+) and PC (GT_-) directions. The work of Fuller et al., (FFN) (Fuller et al. 1980, 1982a, 1982b, 1985), which was based on the independent particle model (IPM), reveals the importance of capture processes to the GT resonance and they calculated capture rates for a wide domain of temperature $10^7 - 10^{11}$ (K) and density $10^1 - 10^{11}$ (g/cm^3) for 226 nuclei with masses in the range 21 to 60. For nuclei, with mass numbers greater than 60, Aufderheide et al., (Aufderheide et al. 1996) updated the work of FFN with the consideration of GT quenching. In a study, El-Kateb et al., (El-Kateb et al. 1994) described the inaccurate placement of GT centroid in the computations done by FFN (Fuller et al. 1980, 1982a, 1982b, 1985) and Aufderheide et al., (Aufderheide et al. 1996). Since, in the massive stars, with intensely hot and dense environment, transitions from the excited states are also notable besides the transitions from the ground states. Therefore, an accurate estimation of the capture rates demands a microscopic calculation of the ground, as well as the excited state GT_\pm strength functions. Two microscopic theories were developed, the proton-neutron quasi-particle random phase approximation (pn-QRPA) theory (Nabi et al. 1999) and the large-scale shell model (LSSM) (Langanke et al. 2000). These theories are considered to be most effective for an accurate estimation of stellar weak rates. The pn-QRPA model uses a large model space of $7\hbar\omega$ for the calculations. Moreover, unlike the LSSM, this model is not based on Brink's hypothesis (Brink 1955), and calculates the GT strength distributions by considering the contributions of all the excited states of parent nuclei separately. These features enhance the reliability of the pn-QRPA theory for computing the stellar weak rates. The reliability and validity of the pn-QRPA model could be evaluated from Ref. (Nabi et al. 2004).

The pn-QRPA theory was employed for the first time by Nabi and Klapdor-Kleingrothaus (Nabi et al. 1999a,

2004) for the computation of the weak decay rates of 709 nuclei (mass number ranging 18-100) for a wide range of stellar temperatures and densities. Later, Nabi and collaborators, further improved the algorithm by refining the model parameters and incorporating the up-to-date experimental data for the calculation of the rates e.g., in (Nabi and Rahman 2005; Nabi et al. 2007, 2008).

In the pre-supernovae development of high-mass stars, weak decay properties of several isotopes of vanadium play an important part (Heger et al. 2001; Aufderheide et al. 1994). Simulation studies of Aufderheide and collaborators show that β decay of $^{50,52-57}\text{V}$ and electron captures on $^{50-55}\text{V}$ are of significant importance as the product of their weak rates and abundances can affect time rate of change of Y_e substantially. Most of the previous studies have focused mainly on the calculations of weak decay properties of stable isotopes (^{50}V and ^{51}V). For example, in Ref. (Nabi et al. 2007), the authors discussed the impact of GT strength distributions on EC rates on ^{50}V . Later, (Rahman et al. 2013) calculated the EC rates on ^{51}V by applying the pn-QRPA theory. The work of (Cole et al. 2012), (Sarriguren 2013) and (Sarriguren 2016) also highlighted the importance of ^{50}V and ^{51}V in astrophysical environment. As future reserach may reveal further astrophysically important vanadium isotopes, it motivated us to calculate the weak decay rates for isotopes of vanadium other than ^{50}V and ^{51}V . Recently, in a study (Shehzadi et al. 2020), we have reported a detailed study of the GT strength distributions, gamma heating rates (λ_γ) and neutrino cooling rates (λ^ν) for a chain of 22 isotopes of vanadium ($^{43-64}\text{V}$) by making use of the deformed pn-QRPA theory. The terrestrial β -decay half-lives of these isotopes were also estimated and were found to be in good accordance with the experimental ones taken from (Audi et al. 2017). The pn-QRPA deduced B(GT) data was also compared with the ones from other models calculations, as well as the experimental data wherever available. A comparison of our computed cooling rates with the ones calculated using the IPM model and LSSM was also presented.

In the current work, we will focus on the computation of the lepton capture weak rates of vanadium isotopes using our recently published B(GT) data. The estimated LC rates are also compared with the previously reported rates of IPM and LSSM. The adopted formalism based on deformed pn-QRPA theory is briefly described in the next section. Section 3 presents the results and discussion on the calculated LC rates of vanadium isotopes. Section 4 covers the conclusions made on the present work.

2 Formalism

The hamiltonian implemented for the deformed pn-QRPA theory has the form

$$H^{\text{QRPA}} = h^{sp} + \nu^{pair} + \nu_{GT}^{pp} + \nu_{GT}^{ph}. \quad (1)$$

here h^{sp} stands for the single-particle (sp) hamiltonian, whose energies and state vectors were estimated by using the Nilsson model (Nilsson 1995). ν^{pair} is the pairing interaction, handled within the BCS approximation, and ν_{GT}^{pp} is the particle-particle (pp) GT force and ν_{GT}^{ph} is the particle-hole (ph) GT force. These forces incorporate the residual interactions for proton-neutron pairs. The force constants for pp and ph interactions were specified by κ and χ , respectively. These constants are parameterized as in (Hirsch et al. 1993)

$$\chi = 23/A \text{ (MeV)}; \quad \kappa = A^{-2/3} \text{ (MeV)}.$$

The same parametrization was used in our recent calculations of B(GT) strength distribution functions and the energy rates of vanadium isotopes (Shehzadi et al. 2020). Among other required parameters of the model are; the Nilsson potential (NP) parameters, which are adopted from Ref. (Nilsson 1995) and the Nilsson oscillator constant was taken as

$$\Omega = 41/A^{1/3} \text{ (MeV)}. \quad (2)$$

The pairing gaps were calculated using the following relation,

$$\Delta_n = \Delta_p = 12/\sqrt{A} \text{ (MeV)}. \quad (3)$$

The nuclear quadrupole deformation β_2 , given by

$$\beta_2 = \frac{125(Q)}{1.44(A^{2/3})(Z)}, \quad (4)$$

Q is the electric quadrupole moment whose values were adopted from (Möller et al. 1995) and A and Z are atomic mass and atomic number, respectively. The Q -values as calculated in Ref. (Audi et al. 2017) were taken.

The basic approach for the calculations of weak decay rates is based on the formalism adopted in the prior work of FNN (Fuller et al. 1980, 1982a, 1982b, 1985). However, in our calculations a microscopic way is adopted to compute the GT strength for capture rates from all parent excited levels. The rates of the lepton capture, from parent n^{th} state to the daughter m^{th} state is given as

$$\lambda_{nm}^{LC} = \left(\frac{\ln 2}{D} \right) [f_{nm}(T, E_f, \rho)] [B(F)_{nm} + (g_A/g_V)^2 B(GT)_{nm}]; \quad L \equiv E, P, \quad (5)$$

In Eq. 5, $B(F)_{nm}$ and $B(GT)_{nm}$ are known as reduced Fermi and GT transition probabilities, respectively and were determined as in (Shehzadi et al. 2020). For present calculations, $D = 6143$ (Hardy et al. 2009) and the ratio g_A/g_V is -1.2694 (Nakamura et al. 2010). The integral taken over total energy, f_{nm} , is the phase space integral (natural units: $c = \hbar = m_e = 1$ were used in its calculations). For lepton capture rates it is given as follows (with upper sign for EC and lower for PC)

$$f_{nm} = \int_{\omega_l}^{\infty} \omega(\omega^2 - 1)^{1/2} (\omega_m + \omega)^2 F(\pm Z, \omega) G_{\mp} d\omega. \quad (6)$$

In this equation, ω is total energy (sum of kinetic and rest mass energies) of electron or positron, ω_m is the total energy of β -decay and ω_l is the total threshold energy for the lepton capture. The G_{\mp} are the Fermi-Dirac lepton distribution function. The Fermi functions $F(\pm Z, \omega)$ are calculated by adopting the method described in (Gove et al. 1971). The total lepton capture rates are given by;

$$\lambda^{LC} = \sum_{nm} P_n \lambda_{nm}^{LC}; \quad L \equiv E, P, \quad (7)$$

Here P_n is the occupation probability of parent excited levels, which obeys the normal Boltzmann distribution. The summation in above equation was taken over set of all parent and daughter nuclei states until the calculated rates were converged.

3 Results and discussions

In this analysis, we have calculated lepton capture rates for twenty two isotopes of vanadium using deformed pn-QRPA model. The mass of nuclides ranges from $A = 43$ to $A = 64$. The list includes the unstable isotopes including the neutron rich isotopes ($^{43-49}\text{V}$ and $^{52-64}\text{V}$), as well as the stable ones (^{50}V , ^{51}V). The calculations have been done for the stellar temperatures ($10^7 - 3 \times 10^{10}$) K and density in the range ($10 - 10^{11}$) g/cm^3 . Our calculated rates have also been compared with the previous calculations done using LSSM and IPM. The calculated lepton capture rates due to $^{43-64}\text{V}$ isotopes are given in Tables 1-6. For space limitations, we have presented the rates only at some selected values of density and temperature. The 1st column of the tables depicts the values of $\log \rho Y_e$ having units of g/cm^3 , where ρ is the baryon density. In the second column, stellar temperature (T_9) are stated in units of 10^9 K. The remaining columns give the pn-QRPA estimated lepton capture rates for our list of

vanadium isotopes in units of s^{-1} . λ^{EC} (λ^{PC}) denotes the weak decay rates because of electron capture (positron capture). As can be observed from Tables 1-6, the values of EC rates rise as the stellar temperature and density increase. It happens as the density of the stellar core increases, the Fermi energy, E_f of the electrons rise which cause an enhancement in electron capture rates. Additionally, an increase in the stellar temperature results in an enhanced occupation probability of excited states of parent nuclei which result in an effective contribution to the sum total of weak decay rates. From tables, it can also be observed that, with the increasing temperature, there is a reduction in the rate of change of EC rates in the high density region ($\log \rho Y_e = 11$). Tables show that, as the stellar temperature rises, the positron capture rates increase. However, in contrast to EC rates, with increasing core density, there is reduction in PC rates. As the core density decreases or the temperature rises (the degeneracy parameter for positrons at this stage becomes negative), high-energy positrons are generated resulting in an increase of positron capture rates. It can also be noted from Tables 1 and 2, that for $^{43-50}\text{V}$ isotopes, PC rates are smaller as compared to the corresponding EC rates by quite a few orders of magnitude. For isotopes having $A \geq 51$, at low and medium densities ($\log \rho Y_e = 3$ and 7), for temperatures ($T_9 \leq 10$), PC rates become bigger than the corresponding EC rates. For higher stellar temperature ($T_9 = 30$), the electron capture rates for $^{51-57}\text{V}$ isotopes become comparable to the PC rates. However, for $A > 57$, as we go to more neutron abundant isotopes, the PC rates are still larger in comparison to the corresponding EC rates by 1-2 orders of magnitude. For high density domain, the EC rates prevail the PC rates and hence the PC rates can be ignored (specially at low temperatures; $T_9 < 30$). The rates at fine temperature-density grid are available and may be requested from the corresponding author.

Next, we present the comparison of our estimated LC rates to those of calculated by LSSM and IPM. We have calculated ratios of our calculated lepton rates to the corresponding rates computed by LSSM and IPM, which have been presented in the form of graphs (see Figures 1 and 2). The ratios (along y-axis) have been plotted against stellar temperature at four different values of density ($\log \rho Y_e = 2, 5, 8, 11$). The left panel of the graphs shows the ratios of our calculated EC/PC rates to the corresponding IPM rates and in the right panel the comparison with respect to LSSM rates has been presented. We had observed that the comparison graphs of several isotopes showed a similar trend and hence we have presented the comparison results only for a few selected cases due to the space consideration.

Figure 1 shows the comparison of EC rates for three selected even-A (odd-A) isotopes, $^{46,48,52}\text{V}$ ($^{49,51,55}\text{V}$) at top (bottom). In case of $^{45-49,53,56}\text{V}$, QRPA-calculated rates are in general greater than the corresponding IPM and LSSM rates at all values of temperature and density. For example, in case of $^{46,49}\text{V}$ (^{48}V), our computed EC rates are bigger than the rates calculated by IPM and LSSM by 1-2 (1-3) orders of magnitude (see Figure 1). This difference in the EC rates estimated using pn-QRPA theory and the other models could be attributed to their different way of computation of GT transition strength contribution from the excited levels. Brink's hypothesis was applied in the calculations of IPM and LSSM for the estimation of excited states GT transition strengths. This hypothesis is based on the assumption that the contribution to GT strengths from the excited levels is comparable to that from the ground state, with the exception that the earlier ones are shifted by the excitation energy of the states. In contrast to this approach, pn-QRPA model adopted a microscopic way of computation of GT transition strength contribution from all the parent's excited levels separately. The summation was then applied over all states of daughter and parent nuclei to evaluate the total capture rates.

In case of $^{50-52}\text{V}$, at lower temperatures and densities, LSSM and IPM EC rates are in general bigger than the corresponding pn-QRPA rates. However, at higher temperatures ($T_9 > 3$) and density, our rates surpass the rates calculated using LSSM and IPM. One of such instance from odd-A nuclei (^{51}V), and one from even-A nuclei (^{52}V), is shown in Figure 1. For ^{51}V , pn-QRPA-computed EC rates are bigger as compared to the IPM (LSSM) rates by up to a factor of 18 (52) at higher temperatures. In case of ^{52}V , at higher temperature and density our estimated rates surpass the IPM and LSSM rates by up to ~ 2 orders of magnitude. In the last row of Figure 1 the rates of ^{55}V are shown. For this isotope, except at high density and low temperatures, our rates are bigger. In addition to the earlier stated different way of calculation of excited level GT strength distribution, some other reasons could contribute to the differences in our and other model's calculated rates. For instance, the calculations of IPM used wrongly placed GT centroid, didn't consider quenching and also suffered from the approximations applied in the calculations of nuclear matrix elements. In case of calculations done by LSSM, some convergence issues were observed as stated in Ref. (Pruet et al. 2003). pn-QRPA theory did not face any such problems and calculates rates in a microscopic manner.

Finally, we move to the comparison of PC rates calculated using different models, which has been presented in Figure 2. It has been observed that generally

at lower temperatures, the IPM and LSSM computed PC rates due to $^{45-50,55}\text{V}$ isotopes are larger than our rates. However at higher temperatures, our rates surpass the LSSM and IPM rates. From this list, the comparison results for one even-A (^{48}V) and two odd-A (^{45}V and ^{49}V) nuclei are shown in Figure 2. For example, in case of ^{48}V , for temperatures ($T_9 < 5$), PC rates computed using LSSM and IPM are greater than our estimated rates by about 1-8 orders of magnitude. Lower the temperature, larger is the difference between the rates. As the temperature rises, the difference between the rates reduces and for temperatures $T_9 \geq 5$, our rates prevail the IPM and LSSM rates by 1-2 orders of magnitude. For ^{45}V , LSSM and IPM rates are bigger than pn-QRPA rates by about a factor two- to three orders of magnitude at temperatures $T_9 \leq 10$. At $T_9 = 30$, QRPA rates exceed the LSSM and IPM rates by factor 2. For the next three cases $^{51,52,54}\text{V}$, at lower temperatures and densities, there is a reasonable comparison between different model calculated rates. At higher temperature QRPA rates get bigger by some factors to an order of magnitude (see for example the results for ^{51}V and ^{54}V). For $^{56-58}\text{V}$, QRPA rates in general exceed the corresponding IPM and LSSM rates at all densities and temperatures by factor of two to an order of magnitude. The results for one such case (^{58}V) are shown in Figure 2. These differences in the PC rates calculated using various models can again be due to the earlier stated reasons. The core-collapse simulators should take notice of the enhancement in our computed LC rates at higher temperatures.

4 Conclusions

We have calculated the lepton capture rates of twenty two isotopes of vanadium using the deformed pn-QRPA theory. The calculations of these rates are based on the GT strength distributions previously reported in Ref. (Shehzadi et al. 2020). The rates were evaluated over a broad temperature ($10^7 - 3 \times 10^{10}$) K and density ($10 - 10^{11}$) g/cm^3 domain. It has been observed that, for lighter V isotopes having $43 \leq A \leq 50$, EC rates are bigger as compared to the corresponding PC rates. In case of heavier isotopes with $A > 50$, the PC rates are bigger in comparison to the EC rates at lower temperatures and densities ($\log \rho Y_e < 11$). However, for $^{51-57}\text{V}$, the EC rates become comparable to PC rates at higher temperatures. At high densities, the PC rates are insignificant in comparison to EC rates.

Our calculated lepton capture rates were also compared with the previously reported LSSM and IPM calculated capture rates. It has been observed that at

higher stellar temperatures, the pn-QRPA computed LC rates are enhanced as compared to the corresponding LSSM and IPM rates by up to 1-2 orders of magnitude. One of the primary reasons which could cause these differences is the use of Brink hypothesis by IPM and LSSM calculations, which is considered a poor approximation in the estimation of GT transition strength from excited states (Misch et al. 2014; Johnson 2015). Our model, on the other hand, treats contribution from excited states microscopically. A larger model space up to 7 major oscillator shells was employed in pn-QRPA calculations. GT strength quenching, and wrong placing of GT centroid in IPM calculations and convergence issues faced by LSSM calculations would also contribute to the differences observed in their and our reported capture rates. From simulation studies, the enhanced LC rates may have an impact on the shock wave energetics and the late stellar evolution phases. We encourage the core collapse simulators to test run their stellar codes to analyze the effect of our enhanced LC rates.

Acknowledgements J.-U. Nabi would like to acknowledge the support of the Higher Education Commission Pakistan through project numbers 5557/KPK/NRPU/R&D/HEC/2016, 9-5(Ph-1-MG-7)/PAK-TURK/R&D/HEC/2017.

Table 1 The pn-QRPA calculated lepton capture rates on $^{43-46}\text{V}$ isotopes at various selected densities and temperatures in stellar environment. $\log \rho Y_e$ has units of g/cm^3 , where ρ is the baryon density and Y_e is the ratio of the lepton number to the baryon number. Temperature (T_9) is given in units of 10^9 K. λ^{EC} (λ^{PC}) are the weak decay rates as a result of electron capture and positron capture, respectively and are given in units of s^{-1} .

$\log \rho Y_e$	T_9	^{43}V		^{44}V		^{45}V		^{46}V	
		λ^{EC}	λ^{PC}	λ^{EC}	λ^{PC}	λ^{EC}	λ^{PC}	λ^{EC}	λ^{PC}
3	1	1.77E-04	4.89E-85	1.61E-04	5.36E-78	8.87E-05	3.64E-68	1.84E-03	1.39E-60
3	3	4.46E-02	5.68E-29	3.77E-02	1.48E-26	1.99E-02	5.07E-24	5.68E-01	2.43E-19
3	5	3.15E-01	1.44E-17	3.34E-01	6.31E-16	1.44E-01	7.23E-15	4.57E+00	6.24E-11
3	10	4.02E+00	1.35E-08	6.46E+00	2.09E-07	2.10E+00	3.00E-07	6.64E+01	2.61E-04
3	30	1.05E+03	6.08E-01	2.80E+03	4.67E+00	7.71E+02	2.24E+00	5.31E+03	5.13E+01
7	1	9.02E-01	7.40E-91	8.34E-01	8.11E-84	4.72E-01	5.51E-74	1.06E+01	2.10E-66
7	3	1.17E+00	1.09E-30	9.93E-01	2.84E-28	5.33E-01	9.77E-26	1.58E+01	4.68E-21
7	5	1.34E+00	2.84E-18	1.43E+00	1.25E-16	6.19E-01	1.43E-15	2.00E+01	1.23E-11
7	10	4.97E+00	1.07E-08	7.98E+00	1.67E-07	2.61E+00	2.39E-07	8.22E+01	2.08E-04
7	30	1.06E+03	6.04E-01	2.82E+03	4.62E+00	7.76E+02	2.22E+00	5.35E+03	5.09E+01
11	1	1.10E+05	1.00E-100	9.48E+04	1.00E-100	1.07E+05	1.00E-100	2.72E+06	1.00E-100
11	3	1.37E+05	3.65E-69	1.13E+05	9.46E-67	1.14E+05	3.25E-64	3.72E+06	1.56E-59
11	5	1.42E+05	1.14E-41	1.43E+05	5.01E-40	1.15E+05	5.74E-39	3.83E+06	4.95E-35
11	10	1.50E+05	1.31E-20	2.12E+05	2.04E-19	1.24E+05	2.92E-19	3.55E+06	2.55E-16
11	30	4.83E+05	8.28E-05	1.13E+06	6.34E-04	4.34E+05	3.04E-04	2.89E+06	6.98E-03

Table 2 Same as Table 1, but for $^{47-50}\text{V}$ isotopes .

$\log \rho Y_e$	T_9	^{47}V		^{48}V		^{49}V		^{50}V	
		λ^{EC}	λ^{PC}	λ^{EC}	λ^{PC}	λ^{EC}	λ^{PC}	λ^{EC}	λ^{PC}
3	1	6.41E-07	1.09E-43	3.94E-05	7.16E-29	3.58E-07	1.17E-19	6.67E-14	4.09E-19
3	3	1.50E-04	3.86E-16	6.25E-02	4.06E-09	2.15E-04	5.55E-08	1.77E-06	4.62E-08
3	5	1.34E-03	2.34E-10	1.03E+00	6.21E-05	3.45E-03	4.42E-05	2.30E-04	1.99E-05
3	10	4.46E-02	1.80E-05	3.40E+01	2.12E-01	1.34E-01	2.44E-02	5.02E-02	8.59E-03
3	30	1.16E+02	3.74E+00	6.98E+03	5.96E+02	1.85E+02	4.92E+01	3.09E+02	6.15E+01
7	1	3.94E-03	1.65E-49	4.63E-01	1.08E-34	4.65E-03	1.77E-25	2.58E-08	6.19E-25
7	3	4.32E-03	7.45E-18	2.19E+00	7.82E-11	8.02E-03	1.07E-09	8.47E-05	8.89E-10
7	5	5.98E-03	4.65E-11	4.80E+00	1.23E-05	1.64E-02	8.75E-06	1.13E-03	3.94E-06
7	10	5.55E-02	1.44E-05	4.25E+01	1.69E-01	1.67E-01	1.95E-02	6.28E-02	6.85E-03
7	30	1.17E+02	3.72E+00	7.03E+03	5.90E+02	1.86E+02	4.88E+01	3.11E+02	6.10E+01
11	1	1.40E+04	1.00E-100	1.27E+06	1.00E-100	4.09E+04	1.00E-100	2.40E+04	1.00E-100
11	3	1.49E+04	2.48E-56	3.50E+06	2.61E-49	4.01E+04	3.56E-48	4.01E+04	2.96E-48
11	5	1.53E+04	1.87E-34	4.23E+06	4.93E-29	3.92E+04	3.52E-29	5.35E+04	1.58E-29
11	10	1.73E+04	1.76E-17	4.46E+06	2.07E-13	3.85E+04	2.38E-14	7.96E+04	8.47E-15
11	30	9.86E+04	5.11E-04	4.63E+06	8.17E-02	1.84E+05	6.76E-03	3.56E+05	8.47E-03

Table 3 Same as Table 1, but for $^{51-54}\text{V}$ isotopes .

$\log \rho Y_e$	T_9	^{51}V		^{52}V		^{53}V		^{54}V	
		λ^{EC}	λ^{PC}	λ^{EC}	λ^{PC}	λ^{EC}	λ^{PC}	λ^{EC}	λ^{PC}
3	1	1.26E-21	1.48E-10	3.86E-32	3.40E-06	6.24E-33	9.86E-08	2.92E-39	1.60E-07
3	3	1.41E-09	2.96E-06	9.12E-11	8.05E-03	6.92E-13	1.35E-04	1.05E-13	3.21E-04
3	5	3.30E-06	7.78E-05	8.51E-06	2.27E-01	5.09E-08	1.54E-03	4.60E-08	4.85E-03
3	10	2.54E-02	2.72E-02	2.47E-01	1.17E+01	1.71E-03	8.13E-02	3.01E-03	2.59E-01
3	30	4.98E+02	2.79E+02	3.72E+03	3.98E+03	1.31E+02	2.82E+02	2.14E+02	5.21E+02
7	1	8.30E-16	2.23E-16	2.55E-26	5.16E-12	4.08E-27	1.49E-13	1.93E-33	2.43E-13
7	3	6.34E-08	5.75E-08	4.73E-09	1.58E-04	3.54E-11	2.64E-06	5.45E-12	6.32E-06
7	5	1.55E-05	1.56E-05	4.31E-05	4.59E-02	2.56E-07	3.13E-04	2.32E-07	9.86E-04
7	10	3.18E-02	2.18E-02	3.10E-01	9.40E+00	2.15E-03	6.50E-02	3.78E-03	2.08E-01
7	30	5.01E+02	2.77E+02	3.76E+03	3.95E+03	1.32E+02	2.81E+02	2.16E+02	5.18E+02
11	1	2.62E+04	1.00E-100	4.93E+06	1.00E-100	2.84E+04	1.00E-100	2.82E+04	1.00E-100
11	3	3.64E+04	1.92E-46	3.62E+06	5.26E-43	2.91E+04	8.81E-45	3.80E+04	2.11E-44
11	5	3.98E+04	6.27E-29	3.30E+06	1.86E-25	2.99E+04	1.26E-27	4.66E+04	3.99E-27
11	10	5.19E+04	2.72E-14	3.40E+06	1.18E-11	3.43E+04	8.09E-14	6.81E+04	2.61E-13
11	30	4.73E+05	3.88E-02	5.27E+06	5.60E-01	2.00E+05	3.92E-02	3.48E+05	7.24E-02

Table 4 Same as Table 1, but for $^{55-58}\text{V}$ isotopes .

$\log \rho Y_e$	T_9	^{55}V		^{56}V		^{57}V		^{58}V	
		λ^{EC}	λ^{PC}	λ^{EC}	λ^{PC}	λ^{EC}	λ^{PC}	λ^{EC}	λ^{PC}
3	1	7.76E-45	7.71E-08	1.94E-40	2.84E-06	1.71E-58	1.16E-06	1.93E-52	3.27E-06
3	3	3.66E-16	7.71E-05	4.29E-14	2.90E-03	1.25E-19	1.39E-03	1.18E-17	9.59E-03
3	5	8.41E-10	6.01E-04	2.96E-08	2.77E-02	2.87E-11	1.30E-02	3.30E-10	1.09E-01
3	10	3.05E-04	1.53E-02	3.10E-03	8.09E-01	2.37E-04	5.42E-01	6.82E-04	2.40E+00
3	30	1.20E+02	4.66E+01	3.09E+02	7.29E+02	1.76E+02	8.79E+02	3.56E+02	1.55E+03
7	1	5.13E-39	1.17E-13	1.28E-34	4.30E-12	1.13E-52	1.76E-12	1.28E-46	4.95E-12
7	3	1.90E-14	1.52E-06	2.23E-12	5.71E-05	6.50E-18	2.74E-05	6.12E-16	1.89E-04
7	5	4.26E-09	1.23E-04	1.50E-07	5.68E-03	1.45E-10	2.66E-03	1.67E-09	2.23E-02
7	10	3.83E-04	1.23E-02	3.89E-03	6.50E-01	2.98E-04	4.37E-01	8.57E-04	1.93E+00
7	30	1.21E+02	4.62E+01	3.12E+02	7.24E+02	1.77E+02	8.73E+02	3.59E+02	1.54E+03
11	1	1.04E+03	1.00E-100	3.27E+03	1.00E-100	8.28E+02	1.00E-100	7.14E+02	1.00E-100
11	3	1.14E+03	5.07E-45	1.19E+04	1.91E-43	8.34E+02	9.12E-44	1.50E+03	6.31E-43
11	5	1.68E+03	5.00E-28	2.38E+04	2.31E-26	9.16E+02	1.08E-26	2.23E+03	9.04E-26
11	10	6.71E+03	1.57E-14	6.11E+04	8.30E-13	6.25E+03	5.57E-13	1.44E+04	2.47E-12
11	30	1.82E+05	6.53E-03	4.82E+05	1.02E-01	2.74E+05	1.24E-01	5.33E+05	2.18E-01

Table 5 Same as Table 1, but for $^{59-61}\text{V}$ isotopes .

$\log \rho Y_e$	T_9	^{59}V		^{60}V		^{61}V	
		λ^{EC}	λ^{PC}	λ^{EC}	λ^{PC}	λ^{EC}	λ^{PC}
3	1	2.94E-67	4.07E-06	3.01E-59	1.46E-06	9.38E-76	3.48E-06
3	3	3.54E-22	4.86E-03	2.50E-19	2.76E-03	8.15E-25	4.14E-03
3	5	1.33E-12	4.56E-02	8.28E-11	2.96E-02	4.36E-14	3.58E-02
3	10	8.34E-05	2.59E+00	7.40E-04	6.08E-01	1.77E-05	6.37E-01
3	30	2.14E+02	4.00E+03	4.70E+02	3.44E+02	9.29E+01	3.52E+02
7	1	1.94E-61	6.17E-12	1.99E-53	2.21E-12	6.19E-70	5.28E-12
7	3	1.84E-20	9.59E-05	1.30E-17	5.45E-05	4.24E-23	8.18E-05
7	5	6.70E-12	9.33E-03	4.19E-10	6.08E-03	2.20E-13	7.36E-03
7	10	1.05E-04	2.08E+00	9.29E-04	4.90E-01	2.23E-05	5.14E-01
7	30	2.16E+02	3.97E+03	4.73E+02	3.41E+02	9.38E+01	3.49E+02
11	1	4.16E+02	1.00E-100	1.04E+02	1.00E-100	8.04E+01	1.00E-100
11	3	5.06E+02	3.20E-43	2.51E+02	1.82E-43	1.19E+02	2.72E-43
11	5	6.25E+02	3.79E-26	4.33E+02	2.47E-26	1.50E+02	2.99E-26
11	10	5.55E+03	2.68E-12	1.18E+04	6.30E-13	4.81E+02	6.64E-13
11	30	3.96E+05	5.73E-01	6.73E+05	4.86E-02	1.34E+05	5.06E-02

Table 6 Same as Table 1, but for $^{62-64}\text{V}$ isotopes .

$\log \rho Y_e$	T_9	^{62}V		^{63}V		^{64}V	
		λ^{EC}	λ^{PC}	λ^{EC}	λ^{PC}	λ^{EC}	λ^{PC}
3	1	4.35E-69	9.38E-06	5.06E-85	1.06E-05	8.47E-81	1.28E-05
3	3	1.73E-22	1.65E-02	1.11E-27	1.40E-02	4.88E-26	3.55E-02
3	5	1.34E-12	1.48E-01	9.23E-16	1.17E-01	1.23E-14	3.51E-01
3	10	1.34E-04	2.65E+00	2.27E-06	2.14E+00	1.16E-05	5.71E+00
3	30	2.48E+02	1.29E+03	2.82E+01	1.59E+03	8.32E+01	1.94E+03
7	1	2.87E-63	1.42E-11	3.34E-79	1.60E-11	5.60E-75	1.94E-11
7	3	9.02E-21	3.26E-04	5.74E-26	2.77E-04	2.53E-24	7.01E-04
7	5	6.79E-12	3.03E-02	4.67E-15	2.40E-02	6.24E-14	7.23E-02
7	10	1.67E-04	2.14E+00	2.85E-06	1.73E+00	1.46E-05	4.61E+00
7	30	2.49E+02	1.28E+03	2.84E+01	1.57E+03	8.38E+01	1.92E+03
11	1	2.66E+02	1.00E-100	8.63E-01	1.00E-100	3.52E+00	1.00E-100
11	3	4.29E+02	1.08E-42	1.07E+00	9.23E-43	1.64E+01	2.33E-42
11	5	4.80E+02	1.23E-25	1.28E+00	9.77E-26	2.43E+01	2.93E-25
11	10	2.58E+03	2.75E-12	4.83E+01	2.23E-12	2.13E+02	5.96E-12
11	30	3.53E+05	1.82E-01	4.03E+04	2.24E-01	1.18E+05	2.77E-01

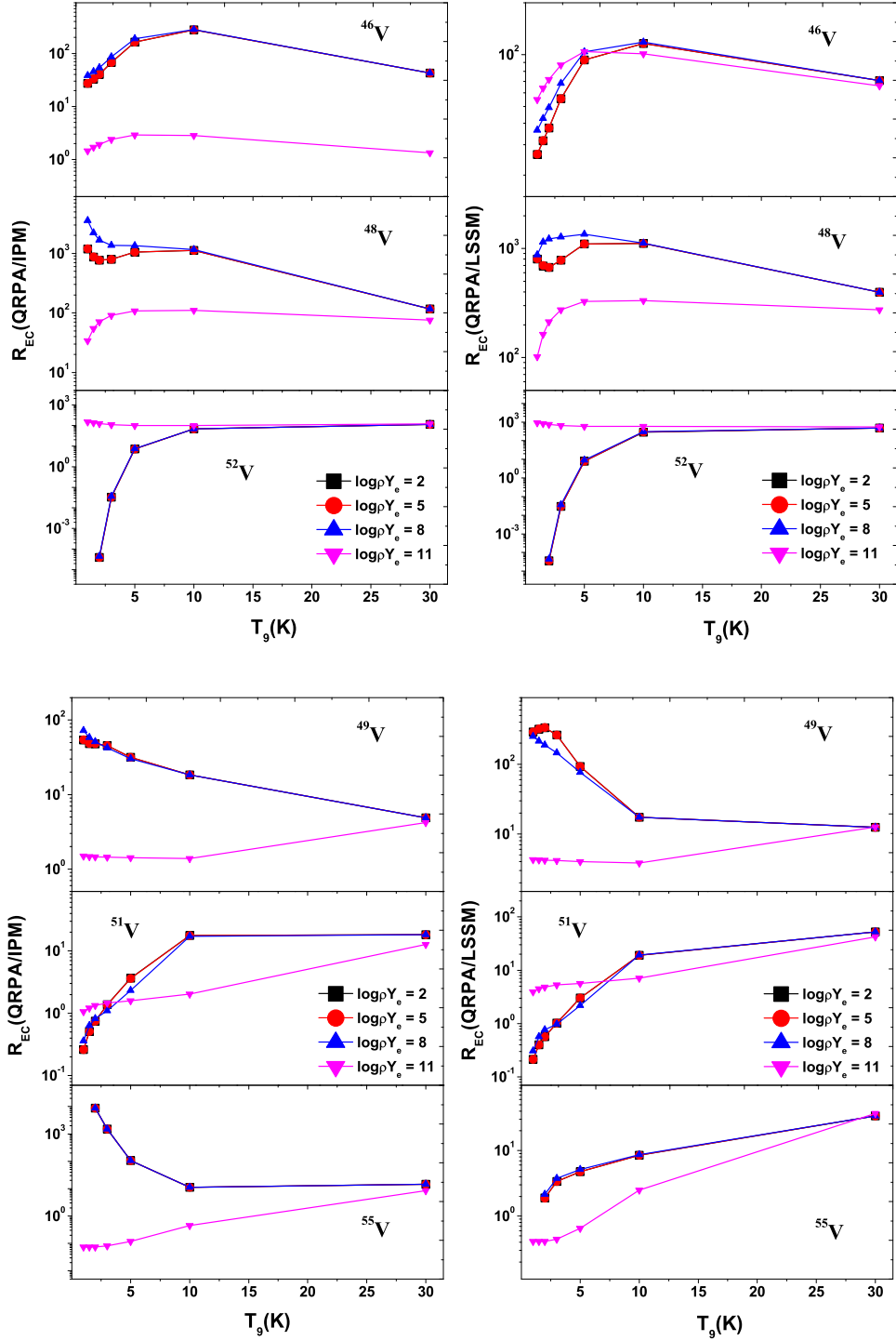


Fig. 1 The comparison of pn-QRPA calculated electron capture rates due to some of even-A (odd-A) vanadium isotopes at top (bottom) with the previous calculations performed by IPM (on left) and LSSM (on right) at different selected densities as a function of stellar temperature. $\log \rho Y_e$ gives the log to base 10 of stellar density in units of g cm^{-3} .

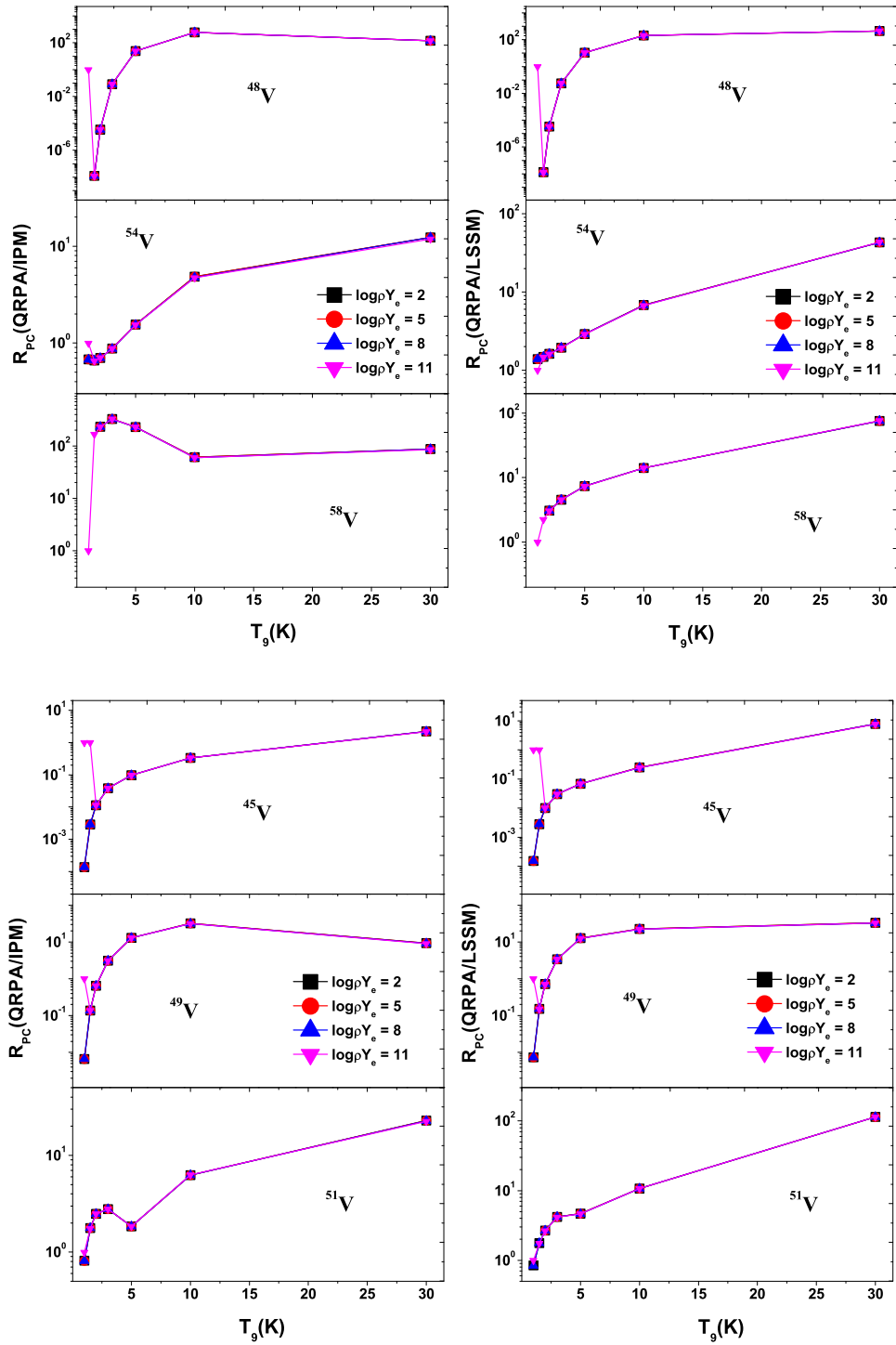


Fig. 2 The comparison of pn-QRPA calculated positron capture rates due to some of even-A (odd-A) vanadium isotopes at top (bottom) with the previous calculations performed by IPM (on left) and LSSM (on right) at different selected densities as a function of stellar temperature. $\log \rho Y_e$ gives the log to base 10 of stellar density in units of g cm^{-3} .

References

- Burbidge, E. M., Burbidge, C. R., Fowler, W. A., Hoyle, F.: *Rev. Mod. Phys.* **29** 547 (1957)
- Bethe, H. A.: *Rev. Mod. Phys.* **62**, 801 (1990)
- Rauscher, T., Heger, A., Hoffman, R. D., Woosley, S. E.: Nucleosynthesis in massive stars with improved nuclear and stellar physics. *Astrophys. J.* **576** 323–348 (2002)
- Busso, M., Gallino, R., Wasserburg, G. J.: Nucleosynthesis in asymptotic giant branch stars: Relevance for galactic enrichment and solar system formation. *Annu. Rev. Astron. Astrophys.* **37** 239–309 (1999)
- Bethe, H. A., Brown, G. E., Applegate J., et al.: *Nucl. Phys. A* **324**, 487 (1979)
- Nabi, J.-U., Rahman, M.-U., Sajjad, M.: *Braz. J. Phys.* **37** 1238 (2007)
- Heger, A., et al.: *Phys. Rev. Lett.* **86** 1678 (2001)
- Langanke, K., Martínez-Pinedon, G.: *Rev. Mod. Phys.* **75** 819 (2003)
- Hix, W.R., Messer, O.E.B., Mezzacappa, A., Liebendörfer, M., Sampaio, J., Langanke, K., Dean, D.J., Martínez-Pinedo, G.: *Phys. Rev. Lett.* **91** 201102 (2003)
- Suzuki, T., Toki, H., Nomoto, K.: *Astrophys. J.* **817**, 163 (2016).
- Nabi, J.-U., Majid, M.: *International Journal of Modern Physics E Vol. 26 No. 3* 1750005 (2017)
- Fuller, G. M., Fowler, W. A., Newman, M. J.: *Astrophys. J. Suppl. Ser.* **42** 447 (1980); **48** 279 (1982a); *Astrophys. J.* **252** 715 (1982b); **293** 1 (1985)
- Aufderheide, M. B., Bloom, S. D., Mathews, G. J., Resler, D. A.: *Phys. Rev. C* **53** 3139 (1996)
- El-Kateb, S., et al.: *Phys. Rev. C* **49** 3128 (1994)
- Langanke, K., Martínez-Pinedon, G.: *Nucl. Phys. A* **673** 481 (2000)
- Nabi, J.-U., Klapdor-Kleingrothaus, H. V.: *Eur. Phys. J. A* **5** 337 (1999)
- Brink, D.: D. Phil. Thesis, Oxford University, Unpublished (1955); Axel, P.: *Phys. Rev.* **126** 671 (1962)
- Nabi J.-U., Klapdor-Kleingrothaus, H. V.: *At. Data Nucl. Data Tables* **88** 237 (2004)
- Nabi, J.-U., Klapdor-Kleingrothaus, H.V.: *At. Data Nucl. Data Tables* **71** 149 (1999)
- Nabi, J.-U., Rahman, M.-U.: *Phys. Lett. B* **612** 190 (2005)
- Nabi, J.-U., Sajjad, M.: *Phys. Rev. C* **76** 055803 (2007)
- Nabi, J.-U., Sajjad, M.: *Phys. Rev. C* **77** 055802 (2008)
- Aufderheide, M. B., Fushiki, I., Woosley, S. E., et al.: *Astrophys. J. Suppl.* **91** 389 (1994)
- Rahman, M.-U., Nabi, J.-U.: *Astrophys Space Sci* **348** 427-435 (2013)
- Cole, A. L., et al.: *Phys. Rev. C* **86**, 015809 (2012)
- Sarriguren, P.: *Phys. Rev. C* **87**, 045801 (2013)
- Sarriguren, P.: *Phys. Rev. C* **93**, 054309 (2016)
- Shehzadi, R. et al.: *Astrophys Space Sci.* 365:3 (2020)
- Audi, G., et al.: *Chin. Phys. C* **41** 030001 (2017)
- Nilsson, S. G.: *Mat. Fys. Medd. Dan. Vid. Selsk* **29** no. 16, (1955)
- Hirsch, M., et al.: *At. Data Nucl. Data Tables* **53** 165-193 (1993)
- Möller, P., et al.: *At. Data Nucl. Data Tables* **59** 185 (1995)
- Hardy, J. C., Towner, I. C.: *Phys. Rev. C* **79(5)**, 055502 (2009)
- Nakamura, K., Particle Data Group *J. Phys. G: Nucl. and Part. Phys.* **37(7A)**, 075021 (2010)
- Gove, N. B., Martin, M. J.: *At. Data Nucl. Data Tables* **10** 205 (1971)
- Pruet, J., Fuller, G. M.: *Astrophys. J. Suppl. Ser.* **149** 189 (2003)
- Misch, G. W., et al.: *Phys. Rev. C* **90** 065808 (2014)
- Johnson, C. W.: *Phys. Lett. B* **750** 72 (2015)